USING PEDESTAL CRATERS AROUND THE MEDUSAE FOSSAE FORMATION, MARS, TO CONSTRAIN EROSION RATES. Joel G. Allen[1] and Tracy K.P. Gregg[1], [1]Dept. of Geology, 876 Natural Sciences Complex, Universitiy at Buffalo, Buffalo, NY 14260, jgallen@buffalo.edu.

Introduction: The Medusae Fossae Formation (MFF) is a locally friable deposit with abundant yardangs [1, 2], located on Mars between 138°– 232°E in the Elysium, Amazonis, and Tharsis regions lies the Medusae Fossae Formation (MFF) (Fig. 1). Using ArcGis and Adobe Illustrator (AI) to analyze locations, diameters, and heights of pedestal craters, we propose to calculate erosion rates of the MFF, thereby giving insight into Mars' recent aeolian history, and possibly into the origin(s) of the MFF [2-9].

Background: The MFF is composed of 3 members (7 units) that appear to be Amazonian in age [2, 11]. For simplicity, we have grouped the MFF into five outcrops (Fig. 1). Outcrop areas range from 1.7 x 10^6 to 3.0 x 10^6 km^2; present outcrop volumes range from 0.135 10^6 – 5.21 x 10^6 km^3. We intprepret the MFF morphology to indicate that the MFF outcrops represent remnants of a much larger, continuous deposit [1, 2, 9-14].

Approach: We propose that pedestal craters are an effective tool for constraining erosion rates of the MFF. Assuming that the height of pedestal craters equals the thickness of MFF material that existed beneath the crater at the time of impact, we can use pedestal craters to constrain the volume of material that has been removed since the crater formed [cf. 15]. Furthermore, the size-frequency distribution of these pedestal craters in relation to the current outcrops of MFF provides rough age constraints. The volume of MFF materials removed in time over the change in area will then provide an approximate erosion rate.

Using THEMIS daytime IR with a resolution of 100 m/px and THEMIS VIS with a resolution of 19m/px, pedestal craters were identified by observing a crater-like depression on a sharply-edged plateau of material [16] (Fig. 2). Diameters of the pedestal craters were measured directly, and pedestal height was calcuated using shadows.

To determine the erosion rate of the MFF, we need to locate the pedestal craters, and measure their distance from the current MFF outcrops. We began by using AI to outline the present MFF outcrops, using available geologic maps and THEMIS daytime IR mosaics [cf. 1, 11]. For each outcrop, this initial outcrop outline was increased incrementally (5-10%) a number of times, and the new outlines were positioned on top of the original outcrop, to model possible paleo-extents of the present MFF outcrops. Pedestal craters falling within these increasingly larger polygons were counted for crater statistics. The topographic high (identified using MOLA) for each outcrop was used as the centerpoint for each, incrementally larger, outline.

Visual inspection of pedestal craters around a given MFF outcrop suggests that the craters can be clustered, and are not equally distributed in all directions from the center of the existing outcrop. For example, pedestal craters are found for a greater distance to the north of the present MFF outcrops than to the south. Therefore, we made a rose diagram reflecting the abundance and distribution of pedestal craters around each outcrop, centered on the topographic high of that outcrop. These rose diagrams controlled how each incrementally larger outcrop outline should be spatially shifted to to best reflect an outcrop's boundaries at different times during the erosion of a once-larger, possibly continuous MFF. We divided the area surrounding the centerpoint into 24 bins of 15° each and counted the number of craters in each direction, assigning a vector to each bin. Upon normalizing the graph to account for unequal areas, we summed the three largest vectors to obtain an single vector. To model possible paleo boundaries for a given outcrop, we shifted each incremental outline in the direction of this vector by a number of kilometers equal to its percent increase from the original outline. In other words, the length of the vector corresponded to a percent; to convert this percent to kilometers, we used the radius of the outcrop in the direction of the vector as equal to 100%. Thus, for the outcrop about the Gordii Dorsum (Fig. 1), with the three stongest vectors averaging 11.0%, the original outline was shifted in the averaged vector's direction 18 km using the minimum outcrop radius (160 km) and 38 km using the radius in the direction of the vector (345 km).

We used three outline shapes for each outcrop: 1) exact –the existing outcrop's boundary, 2) smooth – an approximation of the outcrop's boundary, and 3) ellilptical – based on the shape of the rose-diagram produced for that outcrop. The purpose of the rose-diagram, these multiple outlines, and their shifting was to investigate different erosional patterns that may have modified the MFF.

We will use pedestal crater size-frequency distributions, calculated for the different proposed paleo outlines of the MFF, to constrain the timing of MFF erosion. Pedestal crater height will be used to constrain MFF thickness prior to erosion, and will therefore be used to constrain volumetric erosion rates.

Preliminary Results: Preliminary pedestal crater locations (Fig. 3) around the Gordii Dorsum outcrop using the "exact" outline shape reveal an unequal crater distribution with distance from the present outcrop boundary. This trend suggests a non-linear erosion rate. Future work will examine the size-frequency distribution of pedestal craters around each MFF outcrop, and the spatial distribution of these craters.

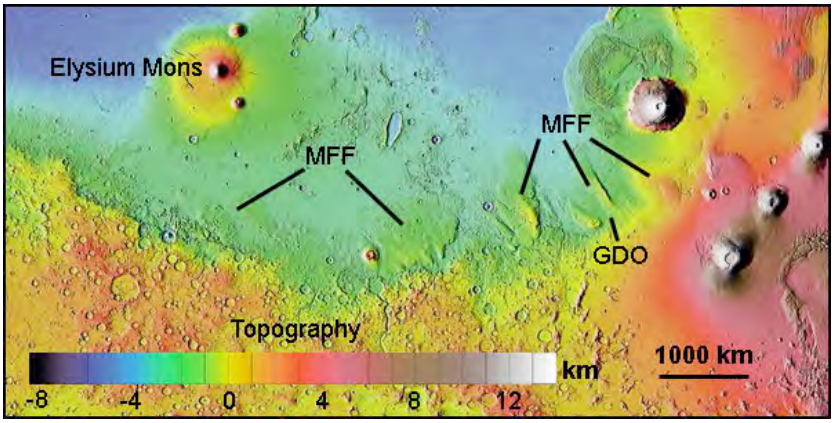

Figure 1. Regional area shown in MOLA data. The MFF spans 138°- 232° E. Lines point to the five outcrops. The Gordii Dorsum outcrop is labeled as GDO. ASU/JPL/NASA

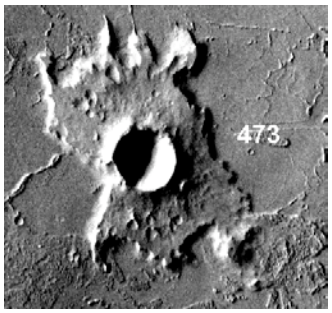

Figure 2. Pedestal Crater #473 from data. Crater diameter is 1.5 km across. Themis VIS image V11801009. ASU/JPL/NASA.

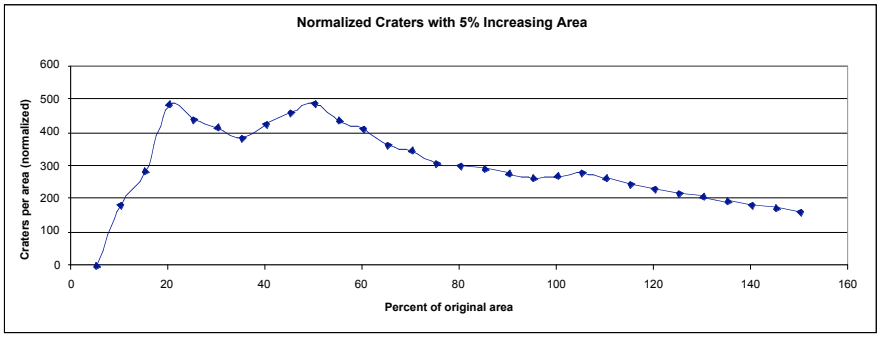

Figure 3. Preliminary results showing pedestal craters N(1.0km).

References: [1] Scott D. H. and Tanaka D. L. (1982) *JGR, 87,* 1179–1190. [2] Bradley B.A. et al. (2001) *JGR, 107, No. E8*, 5058. [3] Ward, A. W. (1979) JGR, 79, 8147-8166. [4] Schultz P. H. and Lutz A. B. (1988) *Icarus*, *73*, 91–141. [5] Head J.W. (2000) *Eos. Trans.*, *AGU 81*, Spring Meet. Suppl., P42A-10. [6] Parker T. J. et al. (1989) *Icarus, 82,* 111-145. [7] Mouginis-Mark P. J. (1993) *LPS XXIV,* 1021-1022. [8] Rice J. W. Jr. (1997) *LPI Contib. 916,* 68. [9] Malin M. C. (1979) *NASA Conf. Publ.* 2072, 54. [10] Shockey K. M. (2005) *LPS XXXVI,* Abstract #1799. [11] Zimbelman J. R. (2001) *AGU 82,* Winter Meet. Suppl., P42A-0560. [12] Tanaka K. L. (2000) *JGR, 91*, 139-158. [13] Sakimoto, S.E.H. et al. (1999) *JGR, 104*, 24,141–24,154. [14] Keszthelyi et al. (2000) *JGR, 105*, 15,027–15,049. [15] Bleacher, J.E. et al. (2003) *JGR 108*:5075. [16] Head J. W. and Roth R. (1976) *LPI, Contrib. 259,* 50-52.